Effect of axial and torsional vibrations on a distributed drill string system

Ulf Jakob F. Aarsnes[1] and Nathan van de Wouw[2]

[1]Norwegian Research Centre (NORCE), Essendropsgate 3, Oslo, Norway
[2]Eindhoven University of Technology, Department of Mechanical Engineering, Eindhoven, The Netherlands

1 Introductino

This paper is concerned with the modelling of drilling systems, involving both the drill string and the cutting process at the bit, towards the goal of analyzing how drilling parameters affect Rate of Penetration (ROP) and stick-slip vibrations. We consider a distributed drill-string and bit-rock interaction model capable of replicating axial and torsional stick-slip as caused by the regenerative effect. We discuss the recent idea that axial stick-slip contributes to higher ROP for a given average hook-load (surface weight on bit). Finally, the model is used to create torsional stability maps.

2 Dimensionless model formulation

We will use a non-dimensional system model so as to express the model by the smallest number of dimensionless parameters derived from the characteristic quantities of the physical system. The detailed model derivation is given in [1].

2.1 Dimensionless PDE model

The model uses the independent spatial and time variables $\bar{t}, \bar{x}$, and the systems dynamics are described as follows. The cut profile, Λ, see Fig. 1, is described by the transport equation [2]

$$\frac{\partial \Lambda(\bar{t}, \theta)}{\partial \bar{t}} + \Omega_b(\bar{t}) \frac{\partial \Lambda(\bar{t}, \theta)}{\partial \theta} = V_b(\bar{t}), \tag{1}$$

where

$$\Lambda(\bar{t}, \theta = 0) = 0, \qquad D(\bar{t}) = \Lambda(\bar{t}, 1), \tag{2}$$

where $D(\bar{t})$ is the depth of cut, and $\Omega_b(\bar{t}), V_b(\bar{t})$ are the angular and axial velocity of the bit. This is used to express the weight- and torque-on-bit, W_b, T_b, as follows:

$$W_b(\bar{t}) = \frac{K_a}{\bar{c}} D(\bar{t}) + W_f g(V_b), \tag{3}$$

$$T_b(\bar{t}) = D(\bar{t}) + \beta W_f g(V_b), \tag{4}$$

where K_a is the axial loop-gain [3]. The second term in (3) denotes the wearflat force component where W_f is the normal force that must be overcome before axial cutting is initiated, while the non-linear function $g(v_b)$ (colloquially referred to as the $g(\cdot)$ non-linearity) is a set-valued map described as (following the description of [4]):

$$g(V_b) = \frac{1 - \text{Sign}(V_b)}{2} = \begin{cases} 0, & V_b < 0 \\ [0, 1], & V_b = 0 \\ 1, & V_b > 0 \end{cases}, \tag{5}$$

where $\text{Sign}(\cdot)$ is the set-valued sign function.

Note the definition of β in (4), which is called the bit-rock interaction number in [5]. β relates the magnitude of changes in the axial wearflat force to changes in the wearflat torque. That is, a large β means that activation of the $g(\cdot)$ nonlinearity in (4) has a large effect on the torque on bit. Consequently, it determines to what degree the wearflat forces influence the torsional dynamics (and the potential occurrence of stick-slip oscillations). The dimensionless axial drill-string dynamics, force, W, and axial velocity, V, are given by

$$\frac{\partial W(\bar{t}, \bar{x})}{\partial \bar{t}} + \frac{\partial V(\bar{t}, \bar{x})}{\partial \bar{x}} = 0 \tag{6}$$

$$\frac{\partial V(\bar{t}, \bar{x})}{\partial \bar{t}} + \bar{c}^2 \frac{\partial W(\bar{t}, \bar{x})}{\partial \bar{x}} = -\bar{k}_a V(t, x), \tag{7}$$

where $\bar{k}_a$ is a linear damping coefficient. The axial boundaryt conditions are

$$W(\bar{t}, \bar{x} = L) = W_b(\bar{t}), \tag{8}$$

while at the topside we use either (9) *or* (10):

$$V(\bar{t}, \bar{x} = 0) = V_0 \tag{9}$$

$$W(\bar{t}, \bar{x} = 0) = W_0, \tag{10}$$

reflecting an imposed axial velocity (rate of penetration), V_0, or imposed axial force (hook-load), W_0, boundary condition, respectively. The dimensionless torsional drill-string dynamics, torque, T, and angular velocity, Ω, are given by

$$\frac{\partial T(\bar{t}, \bar{x})}{\partial \bar{t}} + \frac{\partial \Omega(\bar{t}, \bar{x})}{\partial \bar{x}} = 0 \tag{11}$$

$$\frac{\partial \Omega(\bar{t}, \bar{x})}{\partial \bar{t}} + \frac{\partial T(\bar{t}, \bar{x})}{\partial \bar{x}} = -\bar{k}_t \omega(t, x), \tag{12}$$

with the linear damping coefficient $\bar{k}_t$ and with topside and downhole boundary conditions, respectively, given by

$$\Omega(\bar{t}, \bar{x} = 0) = \Omega_0 \tag{13}$$

$$T(\bar{t}, \bar{x} = L) = T_b(\bar{t}), \tag{14}$$

where $T_b(\bar{t})$ is given by (4).

3 Linearized model description in the Laplace domain

In this section, we state the model description in the Laplace domain which corresponds to the dimensionless model formulation from Section 2. This is the same description as used in [1, 3, 6]. To obtain the Laplace domain model description, we cast the model in perturbation variables, and employ a linearization of the bit rock interaction model in (3),(4). We let the superscripts 'overbar' and 'tilde' denote the steady-state solution and the deviation from this steady-state solution, respectively, for a given variable.

3.1 Drill-string dynamics

Using the Laplace variable $s \in \mathbb{C}$ as the argument to indicate variables in the Laplace domain, we have, for the torsional drill-string dynamics:

$$\frac{\tilde{\Omega}_b}{\tilde{T}_b}(s) = -g_t(s), \qquad g_t(s) = \frac{\tanh\left(s\sqrt{1+\frac{\bar{k}_t}{s}}\right)}{\sqrt{1+\frac{\bar{k}_t}{s}}}, \tag{15}$$

Note that the Laplace transform is performed from the time-domain to the s-domain. Similarly, for the axial dynamics, we have

$$\frac{\tilde{V}_b}{\tilde{W}_b}(s) = -\bar{c}g_a(s), \tag{16}$$

where the transfer function $g_a(s)$ depends on the topside boundary condition (BC):

$$g_a(s) = \begin{cases} \dfrac{\tanh\left(\frac{s}{\bar{c}}\sqrt{1+\frac{\bar{k}_a}{s}}\right)}{\sqrt{1+\frac{\bar{k}_a}{s}}}, & \text{for BC (9).} \\ \dfrac{1}{\sqrt{1+\frac{\bar{k}_a}{s}}\tanh\left(\frac{s}{\bar{c}}\sqrt{1+\frac{\bar{k}_a}{s}}\right)}, & \text{for BC (10).} \end{cases} \tag{17}$$

Here we recall that BC (9) corresponds to constant imposed topside axial velocity, while BC (10) corresponds to constant hook-load.

3.2 Bit rock interaction law

Let the superscripts 'overbar' and 'tilde' denote the steady-state solution and the deviation from this steady-state solution, respectively, for a given variable. E.g., for the depth of cut profile we have $\tilde{\Lambda}(\theta, \bar{t}) = \Lambda(\theta, \bar{t}) - \bar{\Lambda}(\theta)$.

Linearizing (1) around the steady-state profile $\bar{\Lambda}(\theta)$ we obtain

$$\frac{\partial\tilde{\Lambda}(\bar{t},\theta)}{\partial\bar{t}} + \left(\tilde{\Omega}_b(\bar{t})\frac{\partial\bar{\Lambda}(\theta)}{\partial\theta} + \bar{\Omega}\frac{\partial\tilde{\Lambda}(t,\theta)}{\partial\theta}\right) = \tilde{V}_b(\bar{t}). \tag{18}$$

The steady-state gradient of $\bar{\Lambda}(\theta)$ is given by the steady-state velocities $\bar{\Omega}, \bar{V}$ as follows:

$$\frac{\partial\bar{\Lambda}(\theta)}{\partial\theta} = \frac{\bar{V}}{\bar{\Omega}}. \tag{19}$$

Taking the Laplace transform of (18) while using (19), we obtain

$$\tilde{\Lambda}(s,\theta)s + \left(\tilde{\Omega}_b(s)\frac{\bar{V}}{\bar{\Omega}} + \bar{\Omega}\frac{\partial\tilde{\Lambda}(s,\theta)}{\partial\theta}\right) = \tilde{V}_b(s). \tag{20}$$

Hence, we obtain

$$\frac{\partial\tilde{\Lambda}(s,\theta)}{\partial\theta} = \frac{1}{\bar{\Omega}}\left(\tilde{V}_b(s) - \tilde{\Lambda}(s,\theta)s - \tilde{\Omega}_b(s)\frac{\bar{V}}{\bar{\Omega}}\right), \tag{21}$$

$$\tilde{\Lambda}(s,0) = 0. \tag{22}$$

Note that (21) is a linear ODE in θ with initial condition (22), which we can solve to obtain

$$\tilde{\Lambda}(s,\theta) = C_1 \mathrm{e}^{-\theta s/\bar{\Omega}} + \frac{1}{s}\left(\tilde{V}_b(s) - \tilde{\Omega}_b(s)\frac{\bar{V}}{\bar{\Omega}}\right), \tag{23}$$

where C_1 is an integration constant. Enforcing (22) helps to find this integration constant and hence the solution in (23):

$$\tilde{\Lambda}(s,0) = C_1 + \frac{1}{s}\left(\tilde{V}_b(s) - \tilde{\Omega}_b(s)\frac{\bar{V}}{\bar{\Omega}}\right) = 0 \tag{24}$$

$$\implies C_1 = -\frac{1}{s}\left(\tilde{V}_b(s) - \tilde{\Omega}_b(s)\frac{\bar{V}}{\bar{\Omega}}\right). \tag{25}$$

Then we find the Laplace transformed linearized depth of cut as

$$\tilde{D}(s) = \tilde{\Lambda}(s,1) = \frac{1}{s}\left(\tilde{V}_b(s) - \tilde{\Omega}_b(s)\frac{\bar{V}}{\bar{\Omega}}\right)\left(1 - \mathrm{e}^{-s/\bar{\Omega}}\right), \tag{26}$$

and from (3), (4) (noting that the $g(\cdot)$ nonlinearities disappear in the linearized perturbation variables) we obtain:

$$\tilde{W}_b(s) = \frac{K_a}{\bar{c}}\tilde{D}(s), \qquad \tilde{T}_b(s) = \tilde{D}(s), \tag{27}$$

which is consistent with the expressions used in [6, 7, 8, 9].

3.3 Characteristic function

Combining (15), (16) and (26), (27), we obtain the feedback loop generated by the regenerative effect of the rock-cutting process interacting with the drill-string dynamics, see Fig. 2. The stability of this loop can be determined by applying the Nyquist criterion to the characteristic equation [6]:

$$0 = G(s) + 1 \tag{28}$$

$$G(s) = G_a(s) + G_t(s) \tag{29}$$

$$G_a(s) = g_a(s)\frac{K_a}{s}\left(1 - \mathrm{e}^{-s/\Omega_0}\right) \tag{30}$$

$$G_t(s) = -g_t(s)\frac{K_t}{s}\left(1 - \mathrm{e}^{-s/\Omega_0}\right), \tag{31}$$

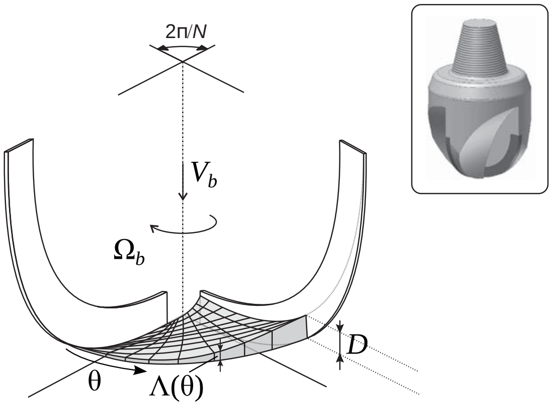

Figure 1: Downhole bit-rock interaction, from [10, 9].

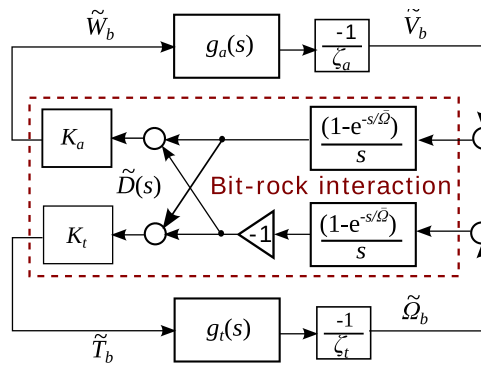

Figure 2: Block diagram of the system.

where key quantities are the axial and torsional loop gain parameters, K_a, K_t. The Nyquist criterion predicts instability if the Nyquist contour of the characteristic function $G(s)$ encircles -1. Note that the torsional loop gain $K_t = \frac{\bar{V}}{\bar{\Omega}}$ is dependent on the steady-state axial velocity $\bar{V}$.

We refer to [6, 3] for details on this kind of analysis. In that analysis it is confirmed that the “well known” approaches of increasing damping (at the top-drive or in the domain) and increasing angular velocity both have a stabilizing effects in terms of linear stability. It is also found that of a low-order lumped-parameter model approach has limitations in evaluating stability.

Finally, in particular for the axial dynamics, achieving stability can be difficult to achieve in practice due to the restrictions on RPM and the difficulty of having sufficient damping in practice. Hence, in practice drilling is usually performed with unstbale axial dynamics and the resulting axial limit-cycle. Hence it is necessary to analyse the resulting behavior by simulating the non-local dynamics.

4 Global Dynamics of the Coupled Axial-Torsional System

In this section, we perform a simulation study of the full coupled model given in Section 2.1.

4.1 Characteristic quantities and simulation setup

Recall that the non-dimensional weight on bit depends on the depth-of-cut D and the $g(\cdot)$ non-linearity as follows:

$$W_b(\bar{t}) = \frac{K_a}{\bar{c}} D(\bar{t}) + W_f g(\bar{t}), \tag{32}$$

and the non-dimensional torque on bit as follows:

$$T_b(\bar{t}) = D(\bar{t}) + \beta W_f g(\bar{t}). \tag{33}$$

We assume a typical value of the relative torsional wave velocity compared to the axial wave velocity of $\bar{c} = 1.6$. Then, there are four remaining characteristic quantities for the torsional and axial feedback loops:

- Nominal axial velocity V_0 or W_0, for BC (9) and (10), respectively,
- Axial loop gain K_a,
- Pseudo reflection coefficients $\eta_a = \mathrm{e}^{-2\frac{\bar{k}_a}{\bar{c}}}, \eta_t = \mathrm{e}^{-2\bar{k}_t}$.

Additionally, there are two characteristic quantities arising from the bit-rock interaction

- Angular top-drive velocity Ω_0.
- β appearing in the torsional bit-rock interaction law, giving the effect of the $g(\cdot)$ nonlinearity on torque on bit, see (33).

Throughout this section, we fix the following parameters:

- $\beta = 0.1$,
- $\eta_t = 0.7$,
- $\eta_a = \pm 0.7$ for BC (9) and (10), respectively.

The three remaining characteristic quantities: Ω_0, K_a, and V_0 or W_0, are considered within representative ranges.

The model is initialized at the equilibrium and then subject to a 15 dimensionless time units square wave added to the weight on bit to perturb the system away from the equilibrium. The simulation is run for 120 time units, and then the existence and magnitude of the torsional limit cycles, and averaged quantities are evaluated over the last 60 time units to assess the steady-state behaviour of the drill-string dynamics.

4.2 Torsional stability, stick-slip occurrence

We introduce the metric

$$M_T = \frac{\Omega_0 - \min_{\bar{t}} \Omega_b(\bar{t})}{\Omega_0}, \tag{34}$$

where $M_T = 1$ indicates a limit cycle that involves torsional stick, i.e., a *stick-slip* limit cycle and $M_T = 0$ indicates a stable steady-state (constant torsional velocity) solution. A constant imposed top-drive velocity is used.

Consider the case of $K_a = 0$, which implies that the linear torsional dynamics are uncoupled from the axial dynamics, i.e., the stability of the torsional dynamics is determined by the torsional part of the characteristic equation

$$G_t(s) = -g_t(s)\frac{1}{s}\frac{\bar{V}}{\bar{\Omega}}\left(1 - \mathrm{e}^{-s/\Omega_0}\right), \tag{35}$$

and the characteristic equation reduces to the torsional term, i.e. $G(s) = G_t(s)$. The corresponding stability map, for $\eta_t = 0.70$ and parametrized in imposed topside velocity V_0, is shown in Fig 3. We expect the non-local torsional dynamics to be dominated by the (non)-occurrence of the torsional instability. This expectation is confirmed in simulations, the result of which is illustrated in Fig. 3 **0)** and **a)** which shows the result of the Nyquist criteria evaluated in the

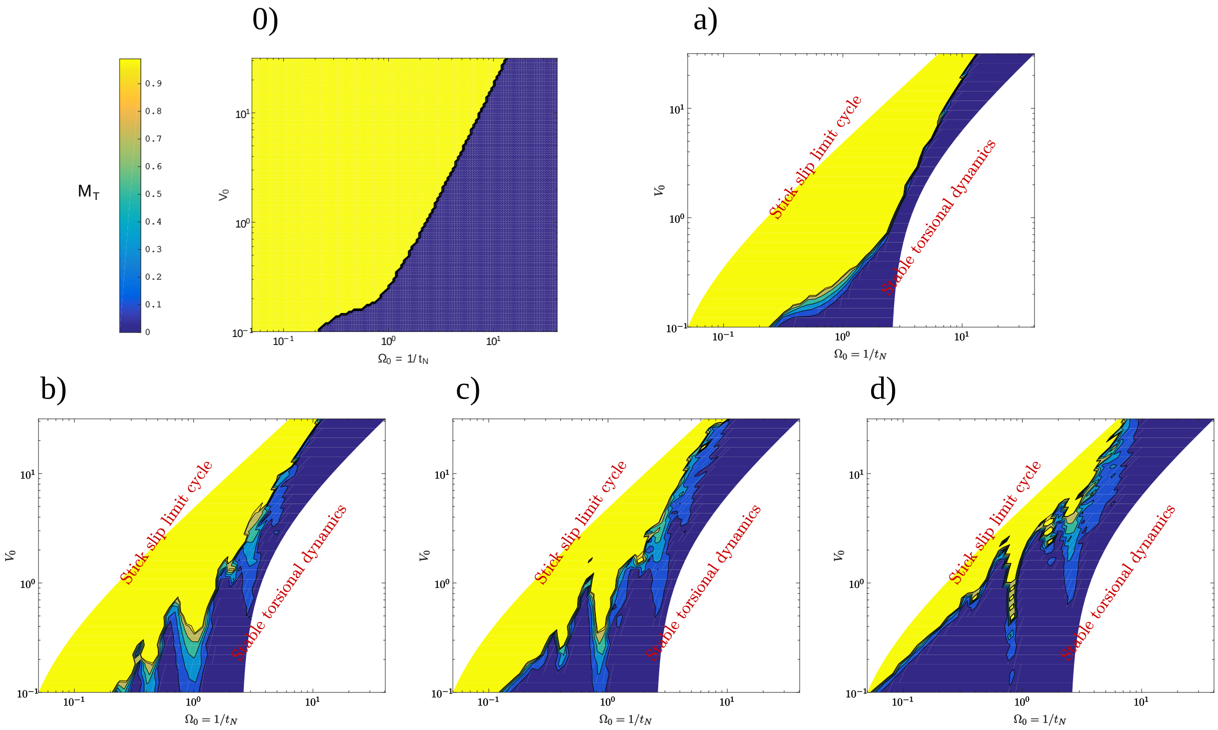

Figure 3: The effect of the axial loop gain, K_a, on the stability of the torsional dynamics where yellow indicates $M_T = 1$, as given in (34), meaning a *stick-slip* limit cycle, and dark blue indicates $M_T < 0.1$ meaning stable torsional dynamics. **0)** Torsional uncoupled dynamics of the drill-string (i.e. $K_a = 0$), derived in the frequency domain using the Nyquist criterion [6]. The other subplots are evaluates from simulations with **a)** $K_a = 0$, **b)** $K_a = 10$, **c)** $K_a = 20$, **d)** $K_a = 40$.

frequency domain and the result of simulating the non-linear model. The occurrence of stick-slip limit cycles in the model closely matches the existence of an unstable pole, as indicated by the Nyquist stability criterion for the case of $K_a = 0$. This is a significant validation of the numerical implementation of the distributed, non-linear model, as it indicates that the behavior is consistent with the stability results of [3] and [6].

Having established the coherence between the previous analytical stability results and the behavior of our simulation model, and, furthermore, established a baseline for behavior of the uncoupled torsional dynamics, we now introduce the axial coupling by setting $K_a > 0$ and evaluate the effect on the M_T metric of (34). The effect of the axial loop gain $K_a > 0$ on the occurrence of stick-slip limit cycles is illustrated in Fig. 3 **b)** – **d)**. The main conclusion from these figures is that increasing the axial loop gain has a *stabilizing* effect on the torsional dynamics. Furthermore, while some of the qualitative properties of the shape of the unstable region are conserved (generally, increasing V_0 has a *destabilizing* effect while increasing Ω_0 has a *stabilizing* effect), the local stability analysis alone is clearly insufficient to evaluate the occurrence of stick-slip oscillations: the greater K_a, the more dissimilar are the local and the nonlocal stability maps. This is related to our final takeaway from this figure: the interaction between the axial non-linear dynamics and the torsional ones results in a more complex topology of the stability map than what is seen in the linear case, the uncoupled case or in the lumped parameter case

[3]. In particular, we note the appearance of *peninsulas* of 'stick-slip limit cycles' along certain RPMs (Ω_0), see Fig. 3. These peninsulas seem to roughly remain along the same RPMs for changing K_a, and indicate the counter-intuitive results that, in specific cases, stick-slip can be avoided by reducing the RPM.

4.3 Constant hook-load

Next, we consider the case of constant imposed hook-load, that is using BC (10). For this case, the equilibrium velocity will be dependent on the axial loop gain K_a.

To understand these stability maps, recall the torsional characteristic equation

$$G_t(s) = -g_t(s)\frac{1}{s}\frac{\bar{V}}{\bar{\Omega}}\left(1 - \mathrm{e}^{-s/\Omega_0}\right), \tag{36}$$

where the torsional nominal loop gain, given by $K_t = \frac{\bar{V}}{\bar{\Omega}}$, is key for stability. Inserting the expression for equilibrium ROP: $\bar{V} = \Omega_0 \frac{W_0 - W_f}{K_a}$, we have

$$K_t \approx \frac{\bar{c}}{K_a}\left(W_0 - W_f\right), \tag{37}$$

where the last approximation comes from noting that typically $\bar{k}_a \ll K_a$. That means that the nominal torsional loop gain might be considered approximately independent of the top drive velocity, Ω_0, while inversely proportional to the axial loop gain K_a, and increasing with weight on bit $W_b - W_f$. In Fig. 4, the stability boundary roughly follows along $W_0 - W_f = 10, 20, 40$ for the cases $W_0 - W_f = 10, 20, 40$ given in **a)**, **b)** and **c)**, indicating that the stability boundary lies around

$$W_0 - W_f = K_a. \tag{38}$$

We note that $K_a = \bar{c}\frac{a\zeta\epsilon L}{EA}N$, where a is bit radius, ζ cutter sharpness, ϵ rock hardness and E, A, L are drill-string elasticity, cross section and length.

4.4 Impact on ROP

Recal that $\bar{V}$ is the equilibrium ROP, that is the ROP with stable dynamics no vibrations for a given weight. We introduce the following metric to evaluate the averaged effect of vibrations on ROP:

$$E_V \equiv \frac{\langle V_0 \rangle}{\bar{V}} = \frac{\langle V_0 \rangle}{\Omega_0}\frac{K_a}{W_0 - W_f}, \tag{39}$$

where $E_V = 1$ when the system is stable, while axial and torsional vibrations can cause E_V to become larger or smaller than one, corresponding to a higher or lower drilling effiency compared to the stable case. Imposing a constant hook-load, using BC (10), a higher $E_V = 1$ corresponds to a higher ROP (V_0) for the given RPM and is considered desirable. E_V obtained in simulations are shown in Fig. 5. Here we see that $E_V > 1$ can be obtained for certain parameter configurations which seems to correspond to an axial instability and vibrations. This makes sense when considering (32) as an axial limit-cycle can reduce work lost to the wearflat force, thereby increasing the cutting component [11, 12, 13] We also see a founder-effect fot high WOB, probably casused by stick-slip.

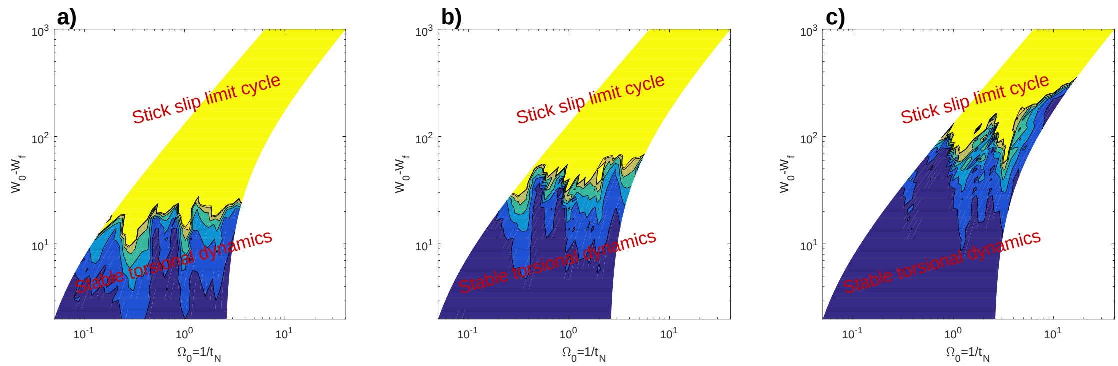

Figure 4: Occurrence of stick-slip for imposed constant hook load. Yellow indicates $M_T = 1$, as given in (34), meaning a *stick-slip* limit cycle, and dark blue indicates $M_T < 0.1$ meaning stable torsional dynamics, with **0)** $K_a = 0$, **a)** $K_a = 10$, **b)** $K_a = 20$, **c)** $K_a = 40$.

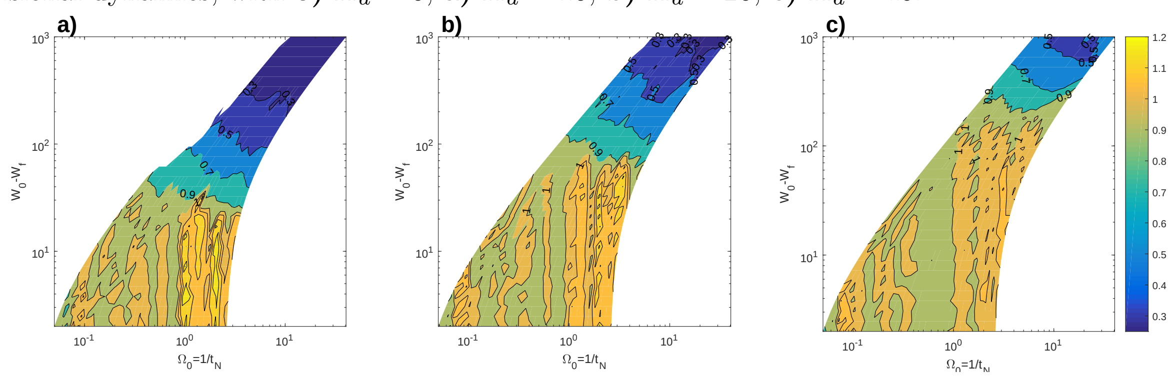

Figure 5: Drilling efficiency parametrized in $E_V = \frac{V_0}{\Omega_0}\frac{K_a}{W_0 - W_f}$ for: **a)** $K_a = 10$, **b)** $K_a = 20$, **c)** $K_a = 40$. We see vibrational founder occurring for high WOB, probably casused by stick-slip.

5 Conclusion

In this paper, we have considered a distributed axial-torsional drill-string model with a rate-independent bit-rock interaction law to study the occurrence of axial and torsional self-excited vibrations as caused by the regenerative effect induced by the bit-rock interaction.

We find that The occurrence of torsional stick-slip roughly matches the stability predictions of the linearized torsional loop and increasing the RPM, Ω_0, and increasing the axial loop gain, thus the severity of the axial instability, has a stabilizing effect on torsional dynamics. Based on the simulation results, we proposed the stability heuristic that the stick-slip instability occurs when the non-dimensional weight on bit, subtracted the wearflat component, is greater than the axial loop gain. We also find that the axial vibrations can improve drilling efficiency, while torsional vibrations (unsurprisingly) reduces efficiency.

References

[1] Ulf Jakob F. Aarsnes and Nathan van de Wouw. Axial and torsional self-excited vibrations of a distributed drill-string. *Journal of Sound and Vibration*, 444(March):127–151, 2019.

[2] Sunit K Gupta and Pankaj Wahi. Global axial–torsional dynamics during rotary drilling. *Journal of Sound and Vibration*, 375:332–352, aug 2016.

[3] Ulf Jakob F. Aarsnes and Nathan van de Wouw. Dynamics of a distributed drill string system: Characteristic parameters and stability maps. *Journal of Sound and Vibration*, 417:376–412, mar 2018.

[4] B. Besselink, N. van de Wouw, and H. Nijmeijer. A Semi-Analytical Study of Stick-Slip Oscillations in Drilling Systems. *Journal of Computational and Nonlinear Dynamics*, 6(2):021006, 2011.

[5] Thomas Richard, Christophe Germay, and Emmanuel Detournay. Self-excited stick-slip oscillations of drill bits. *Comptes Rendus Mécanique*, 332(8):619–626, aug 2004.

[6] Ulf Jakob Flø Aarsnes and Ole Morten Aamo. Linear stability analysis of self-excited vibrations in drilling using an infinite dimensional model. *Journal of Sound and Vibration*, 360:239–259, jan 2016.

[7] K. Nandakumar and Marian Wiercigroch. Stability analysis of a state dependent delayed, coupled two DOF model of drill-string vibration. *Journal of Sound and Vibration*, 332(10):2575–2592, may 2013.

[8] Tamás Insperger, Gábor Stépán, and Janos Turi. State-dependent delay in regenerative turning processes. *Nonlinear Dynamics*, 47(1-3):275–283, nov 2006.

[9] Thomas Richard, Christophe Germay, and Emmanuel Detournay. A simplified model to explore the root cause of stickslip vibrations in drilling systems with drag bits. *Journal of Sound and Vibration*, 305(3):432–456, aug 2007.

[10] Christophe Germay, Vincent Denoël, and Emmanuel Detournay. Multiple mode analysis of the self-excited vibrations of rotary drilling systems. *Journal of Sound and Vibration*, 325(1-2):362–381, aug 2009.

[11] Ulf Jakob F. Aarsnes and Nathan van de Wouw. Effect of shock subs on self-excited vibrations in drilling systems. *Journal of Petroleum Science and Engineering*, 181:106217, oct 2019.

[12] Roeland Wildemans, Arviandy Aribowo, Emmanuel Detournay, and Nathan van de Wouw. Modelling and dynamic analysis of an anti-stall tool in a drilling system including spatial friction. *Nonlinear Dynamics*, 98(4):2631–2650, 2019.

[13] Thijs Vromen, Emmanuel Detournay, Henk Nijmeijer, and Nathan van de Wouw. Dynamics of drilling systems with an antistall tool: effect on rate of penetration and mechanical specific energy. *SPE Journal*, 2019.